SPH MODELLING OF METAL FORGING

Joseph HA, Paul W. CLEARY and Mahesh PRAKASH

CSIRO Mathematical and Information Sciences, Clayton, Victoria 3169, AUSTRALIA

ABSTRACT

In solid metal forming processes, such as forging, large distortions in the material present challenging problems for numerical simulation using grid based methods. Computations invariably fail after some level of distortion is reached unless suitable re-meshing is implemented to cope with the mesh distortion arising from the material deformation. The issue of mesh distortion and the subsequent re-meshing are topics of much research for grid based methods. These problems can be overcome by using meshless numerical methods. Smoothed Particle Hydrodynamics (SPH) is used to model large scale deformation in metal forging in a number of representative work pieces. The test problems demonstrate the ability of SPH to model elastic-plastic solid mechanics problems. SPH also offers advantages in direct prediction of defects because of its ability to advect the material history with the particles.

NOMENCLATURE

a characteristic length
g   gravity
m mass
P pressure
t time
v   velocity
ρ density

INTRODUCTION

The use of simulation software in the forging community has become increasingly common. The main reasons for carrying out forging simulations include:

- Optimisation of number of operations to form the component.
- Optimisation of the size and shape of the blank.
- Optimisation of material flow.
- Prediction of forging defects such as fold, wrinkle and under fill.

In metal forming processes, in particular metal forging, material distorts substantially, which presents difficulties for the numerical simulation of the process. When the metal-forging process is analysed by the finite element methods using isoparametric elements, the analysis fails after some level of distortion (Cho and Yang, 2000). In finite element analysis, the deformation of each element must be evaluated after each load increment. Deformation at any point in each element is evaluated from the nodal point displacement of its nodes, which is related to the change of natural co-ordinates of each nodal point. Thus, the Jacobean operator at each load increment must also be evaluated. When severe mesh distortions occur, the Jacobian determinant becomes negative terminating the computation (Li and Belytschko, 2001). As a result, the deformation, strain, and equivalent nodal force which are in balance with the external load can no longer be evaluated. These problems can be avoided by using a meshless method such as Smoothed Particle Hydrodynamics. This paper discusses the result of our effort to apply SPH to model metal forging. In the next section, the SPH method is presented. A number of simulation results are then presented to demonstrate the attractiveness of the SPH method to model metal forging.

THE SPH METHOD

A brief summary of the SPH method is presented here. For more comprehensive details one can refer to Cleary, et al. (2005). The interpolated value of a function A at any position **r** can be expressed using SPH smoothing as:

$$A(\mathbf{r}) = \sum_b m_b \frac{A_b}{\rho_b} W(\mathbf{r} - \mathbf{r}_b, h) \qquad (1)$$

The sum is over all particles b within a radius $2h$ of **r**. Here $W(\mathbf{r}, h)$ is a C^2 spline based interpolation or smoothing kernel with radius $2h$, that approximates the shape of a Gaussian function but has compact support. The gradient of the function A is given by differentiating the interpolation equation (1) to give:

$$\nabla A(\mathbf{r}) = \sum_b m_b \frac{A_b}{\rho_b} \nabla W(\mathbf{r} - \mathbf{r}_b, h) \qquad (2)$$

Using these interpolation formulae and suitable finite difference approximations for second order derivatives, one is able to convert parabolic partial differential equations into ordinary differential equations for the motion of the particles and the rates of change of their properties.

Continuity Equation

From Monaghan (1992), the SPH continuity equation is:

$$\frac{d\rho_a}{dt} = \sum_b m_b (\mathbf{v}_a - \mathbf{v}_b) \bullet \nabla W_{ab} \qquad (3)$$

We denote the position vector from particle b to particle a by $\mathbf{r}_{ab} = \mathbf{r}_a - \mathbf{r}_b$ and let $W_{ab} = W(\mathbf{r}_{ab}, h)$ be the interpolation kernel with smoothing length h evaluated for the distance $|\mathbf{r}_{ab}|$. This form of the continuity equation is Galilean invariant (since the positions and velocities appear only as differences), has good numerical

conservation properties and is not affected by free surfaces or density discontinuities. The use of this form of the continuity equation is very important for predicting free surface flows of the present kind.

Momentum Equation

The momentum equation used for the elasto-plastic deformation of the solids is:

$$\frac{dv^i}{dt} = \frac{1}{\rho_s}\frac{\partial \sigma^{ij}}{\partial x^j} + g^i \; , \tag{7}$$

where σ is the stress tensor which can be written as:

$$\sigma^{ij} = -P_s \delta^{ij} + S^{ij} \; , \tag{8}$$

and P_s is the pressure and S is the deviatoric stress. Assuming Hooke's law with shear modulus μ_s, the evolution equation for the deviatoric stress S (see Gray, et al., 2001) is:

$$\frac{dS^{ij}}{dt} = 2\mu_s\left(\dot{\varepsilon}^{ij} - \frac{1}{3}\delta^{ij}\dot{\varepsilon}^{ij}\right) + S^{ik}\Omega^{jk} + \Omega^{ik}S^{kj} \tag{9}$$

where

$$\dot{\varepsilon}^{ij} = \frac{1}{2}\left(\frac{\partial v^i}{\partial x^j} + \frac{\partial v^j}{\partial x^i}\right) \tag{10}$$

and

$$\Omega^{ij} = \frac{1}{2}\left(\frac{\partial v^i}{\partial x^j} - \frac{\partial v^j}{\partial x^i}\right) \tag{11}$$

is the rotation tensor. The following equation of state is used:

$$P_s = c_0^2(\rho_s - \rho_{s0}) \tag{12}$$

where ρ_{s0} is the reference density. The subscript s in the above symbols refers to the solid state. The bulk modulus is $K = \bar{\rho}_s c_0^2$ and the Poisson ratio v_s is:

$$v_s = \frac{(3K/\mu_s - 2)}{2(3K/\mu_s + 2)} \tag{13}$$

Equation of state and speed of sound

The SPH method used here is quasi-compressible with the pressure calculated from the particle density using an equation of state:

$$P_s = c_0^2(\rho_s - \rho_{s0}) \tag{5}$$

where P_0 is the magnitude of the pressure and ρ_0 is the reference density. For liquid metals we use $\gamma = 7$. This pressure is then used in the SPH momentum equation (4) to give the particle motion. The pressure scale factor P_0 is given by:

$$\frac{\gamma P_0}{\rho_0} = 100V^2 = c_s^2 \tag{6}$$

where V is the characteristic or maximum fluid velocity. This ensures that the density variation is less than 1% and the flow can be regarded as incompressible.

Plasticity model

The plasticity model used is a radial return plasticity model originally proposed by Wilkins (1964). The trial stress S_{Tr}^{ij} is the deviatoric part of the stress calculated assuming that the initial response is elastic,

$$S^{ij} = \alpha S_{Tr}^{ij} \tag{14}$$

where S^{ij} is the final deviatoric stress at the end of a time-step and α is a proportionality constant given by:

$$\alpha = \left(1 - \frac{3\mu_s \Delta\bar{\varepsilon}^p}{\bar{\sigma}^{Tr}}\right) \tag{15}$$

with $\sqrt{\frac{2}{3}}\bar{\sigma}^{Tr}$ being the magnitude of the trial deviatoric stress and $\Delta\bar{\varepsilon}^p$ being the increment in equivalent plastic strain:

$$\Delta\bar{\varepsilon}^p = \frac{\bar{\sigma}^{Tr} - \sigma_y^n}{3\mu_s + H} \tag{16}$$

where σ_y^n is the final yield stress and H is the hardening modulus. The stress update is completed by adding the deviatoric and mean stress as given in equation (8). The plastic strain is incremented as:

$$\bar{\varepsilon}^p = \bar{\varepsilon}^p + \Delta\bar{\varepsilon}^p \tag{17}$$

History Dependent Properties of the Metal

Each SPH particle represents a specific volume of metal and carries that information with it. This is a critical attribute of the Lagrangian methods. This means that information on the precise state of each piece of metal can be known at all times and the history of each piece of metal is built into the particle data. This provides significant capability to track properties such as:

- Cumulative plastic strain
- Damage (which is a volume averaged local measure of cracking) leading to fracture prediction
- Metal composition (including tracking multiple metals or metal composites) and trapped gas
- Metallic phase and microstructure
- Grain flow
- Surface oxide

Some or all of these properties can then be used to feed back into the flow dynamics using suitable rheology models.

FORGING MODELLING USING SPH

In this section, a number of 2D and 3D forging examples are presented to demonstrate the attractiveness of SPH in modelling metal forging. Although the 2D examples are not realistic, they serve to illustrate the various issues involved in forging clearly. It also serves to highlight one of the attractive features of SPH which is that there is no dimensional difference between 1D, 2D and 3D as far as computer coding for their implementation is concerned.

Bulk Modulus (GPa)	70.0
Shear Modulus (GPa)	27.0
Initial Yield Stress (MPa)	55.2
Hardening Modulus (MPa)	1.67
Density (kg/m$^{3)}$)	2700.0

Table 1: Properties of Al alloy A6061 used for forging.

The base material properties used in forging simulations presented in this paper are given in Table 1. For the 3D forging examples the moduli and yield stress are scaled down by a factor 100 to speed the calculations.

2D Numerical Examples

Figure 1 shows a simple example of impression die forging where two dies are brought together and the work piece undergoes deformation until it takes on the shape of the cavity formed by the dies. The dies are both 1 m wide. The upper die is 0.2 m high and the lower die is 0.4 m. The work piece is 0.56 m wide by 0.4 m high. The upper moving die is located above the work piece which is sitting on the stationary lower die. The upper die is subject to an applied force of 4.0×10^5 N and accelerates downwards. In this SPH simulation, 3027 particles of 10 mm diameter are used to model the dies and work piece.

In Figure 1, the particles are coloured by the plastic strain, and show the deformation process for the work piece and the locations of high strain. The force from the upper die begins to be felt by the work piece at 10 ms. As the top die moves further down, plastic deformation of the work piece occurs in the regions near the two contact points with the lower die. The deformation is mainly sideways forcing solid metal into the side cavities. The central part of the work piece moves steadily down into the open region of the bottom die with little deformation. After about 40 ms, there are high deformations found in all the work piece material that is touching or near the contacts with the lower die. The central section of the work piece continues to move unimpeded down into the lower die space. Moderate plastic strains are now experienced by all the material above the high strain contacts as this material is progressively forced sideways.
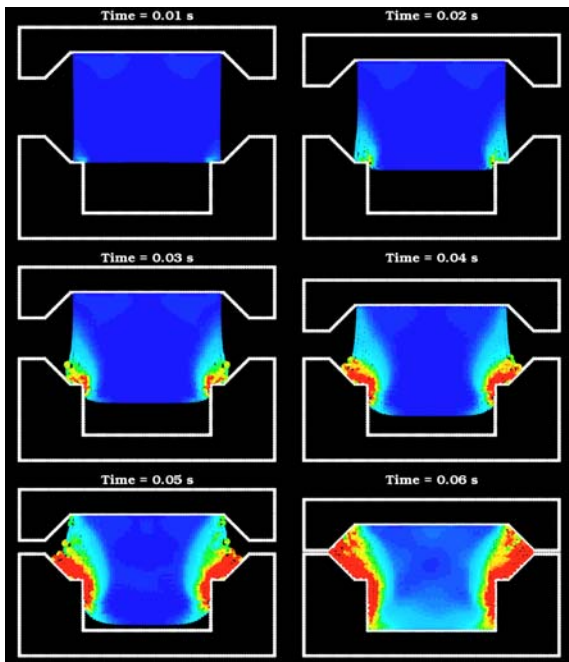

Figure 1: Simple forging example using SPH. The particles coloured by the values of plastic strain with blue for 0.0, green for 0.5 and red for 1.0.

By 50 ms, the outer edges of the contact regions between the work piece and the lower die have moved outward almost to the opening between the dies. All the metal being forced into these side gaps between the dies has now experienced medium to high levels of plastic deformation. The free surface of the work piece at the bottom in the middle of the die has now become curved as the resistance to flow along the walls slows the outer material. The forging operation is completed soon after 60 ms and the work piece takes on the shape of the cavity formed by the upper and lower dies. The high plastic strain is concentrated in the side regions of the forging. High strain is important since it affects material properties and mechanical performance of the die and the creation and migration of grain scale defects. The plastic strain is moderate along the bottom of the forging and low across the top and throughout much of the middle regions.
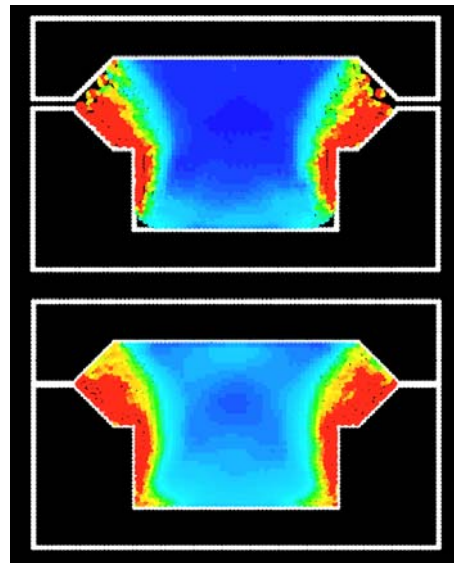

Figure 2: Effect of different applied force – (top) inadequate applied force of 3×10^5 N; (bottom) good forging force of 8×10^5 N.
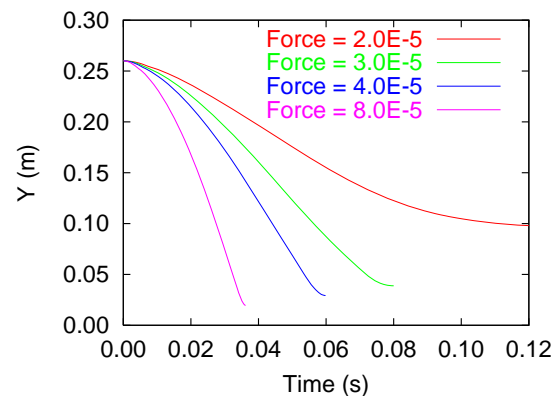

Figure 3: Position of the top die as a function of time for different applied forging forces.

The magnitude of the applied force used to move the top die is an important process parameter. If the applied force is lowered to 3.0×10^5 N, then it is not sufficient to completely close the dies. The incomplete forging is shown in Figure 2 along with the final forging when using

3

a more adequate forging force of 8.0×10^5 N. Incomplete forging due to insufficient force is one of the simplest forging defects to predict. In this case, a force of 4.0×10^5 N is sufficient. The use of larger forces than 4.0×10^5 N just affect time required to forge a component. In Figure 3, the motion of the top die with time for different applied force is shown for both inadequate and adequate forging forces. The figure shows that the forging operation took 0.06 s if the applied force is 4.0×10^5 N but only 0.036 s if the applied force is 8.0×10^5 N. Cases where the y value does not reach 0.025 m indicate that the die has not fully closed and that the force applied is inadequate.

One potential use of simulation software for forging is to reduce material waste and to predict the correct size of the work piece to be forged. In Figure 4, the results of using the wrong size for the work piece leading to incomplete filling of the die is shown in frame a and to flashing is shown in frame b. Incomplete filling is a defect that requires the part to be discarded. Flashing occurs when metal is forced, in a thin layer, out between the two dies. If the flashing is thin, this can be removed by trimming, but this adds costs and should be minimised. If the flashing is thick enough, then physical removal can damage the forging as the mechanical strength of the thick flashing becomes significant. The correct prediction of work piece size using simulation software will avoid potential forging problems arising from the use of incorrect size for the work piece.
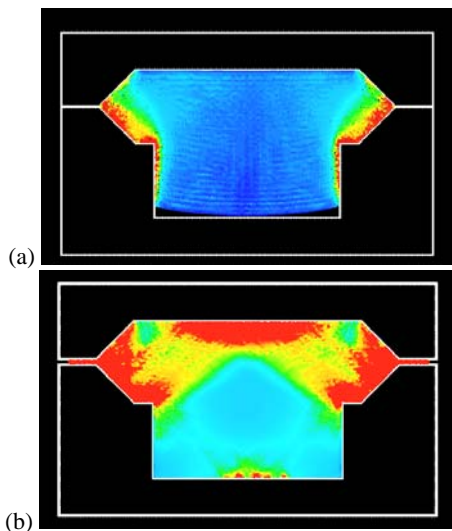

(a)

(b)

Figure 4: Forging defects due to improper size of the work piece, (top) incomplete filling due to a work piece that is too small, and (bottom) flashing of excess material between the top and bottom dies.

One of the advantages of forging over other manufacturing processes such as casting is to be able to control the grain direction in the metal microstructure of the manufactured part through control of the applied stresses. It is useful to colour the initial work piece in horizontal strata. This allows us to monitor the deformation of regions and the changes that occur to the strata as the work piece deforms under the applied force from the top die.

Figure 5 shows the same forging using two different work hardening moduli. The material is coloured in strata to show the difference in the deformation patterns. The effects of deformation on the grain microstructure can be deduced from these patterns. The hardening modulus used on the left is 0.0167 MPa whilst on the right we use 1.67 MPa. For the case of lower hardening modulus, the surface of the blank remains smooth during compression. For metal with a higher hardening modulus, the surface of the blank becomes rippled with small scale rounded structures protruding from the surface. These lead to lap formation where surface material (including oxide) is folded back into the forging leading to regions that are mechanically weaker. These are issues one might expect in forging harder metals such as titanium.
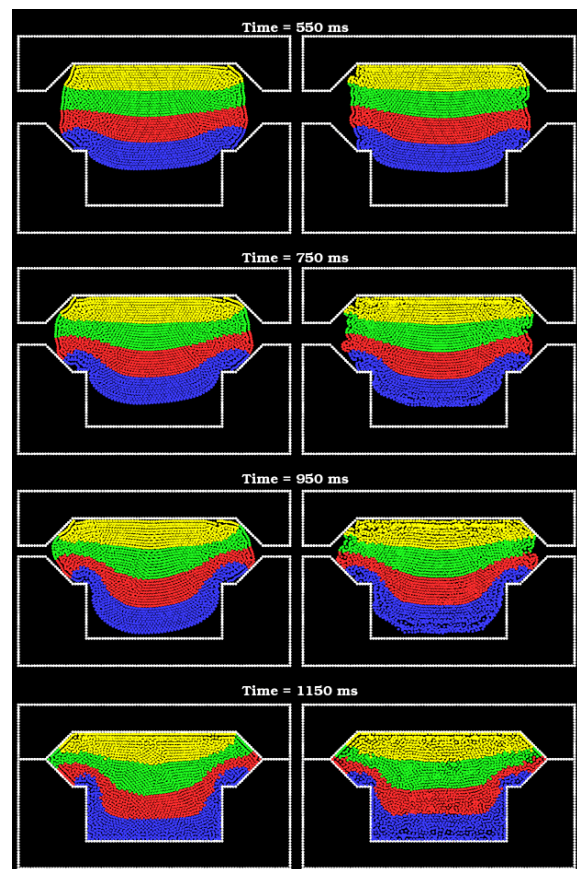

Figure 5: Effect of hardness parameter on material deformation under compaction. The hardening modulus for the right column is 100 times that of the left column. Particles are coloured in initially horizontal strata to show the pattern of metal deformation.

There are also differences in the filling for the two cases, specifically relating to the distribution of the blue material. In the core of the forging, the strata boundaries are flatter and more horizontal indicating that the deformation is more localised near the initial contact points with the lower die. Under the compression from the top die, the blue harder material near the contact points pushes straight down (refer to 750 ms and 950 ms frames of Figure 5) whereas the softer material bulges down smoothly. This could be interpreted as there being greater resistance to bending for the harder material than the softer material.

4

This example also demonstrates prediction of one of the issues relating to improper design of the die, that being the ability of the work-piece to move laterally within the die during loading, leading to asymmetry in forged components. Here the work-piece moves slightly to the right as it is being pushed into the die, leading to an asymmetric filling pattern with the left hand side moving faster than the right.

3D Numerical Examples

Next we present realistic 3D SPH forging simulations representative of real components. Figure 6 shows two views of the geometry of the die for forging the first component. The geometry does not include the four tubes of radius 0.02 m extending from the four arms of the die that guide the motion of the pistons for compressing the work piece into the shape of the die. The length of each of the four arms of the die is 0.075 m. The radius of each arm is 0.02 m and the radius of the enlarged section of the arm is 0.03 m. A cylindrical blank of length 0.64 m and radius 0.018 m is placed in the die at the start of forging. In the SPH simulation, 31952 particles of 4 mm are used to represent the blank, die and pistons.
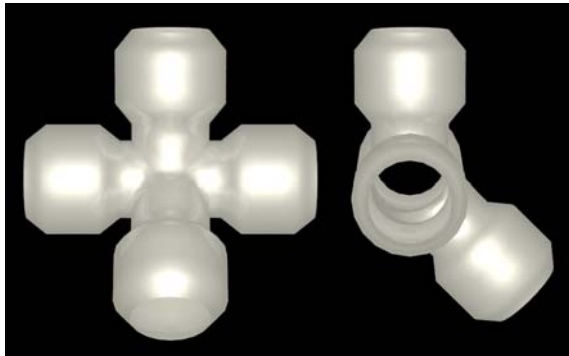

Figure 6: Two views of the geometry of the die for forging component 1.

Figure 7 shows the different stages of forging. The particles in the blank are coloured in 10 vertical strata to allow the deformation to be tracked. As the blank is compressed by the two horizontal pistons, more material is pushed into the die. At 1 s, three bulges are observed. At 2 s, material begins to fill the two vertical arms of the die. The wider diameter sections of the horizontal arms are now almost filled. Up to 2 s, the material flow is fairly symmetric with respect to a vertical plane through the middle of the die. At 2.25 s, the material motion upwards and downwards in the vertical arms is halted and the metal is forced sideways at the ends. At 2.5 s, the metal in the vertical arms is being pushed sideways towards the side walls and the die is almost full. Forging is completed at 2.8 s with all the voids filled.

Figure 8 shows the geometry of the second component. It consists of 4 cylinders of different radii placed concentrically on top of one another. The radii are 0.04 m, 0.06 m, 0.08 m and 0.12 m, respectively. In the same order, their heights are 0.03 m, 0.03 m, 0.05 m and 0.1 m. Each of the 8 pins is 25 mm high and 7.5 mm radius. In the simulation, 51,283 SPH particles of 4 mm were used to represent the die, piston and the cylindrical blank.
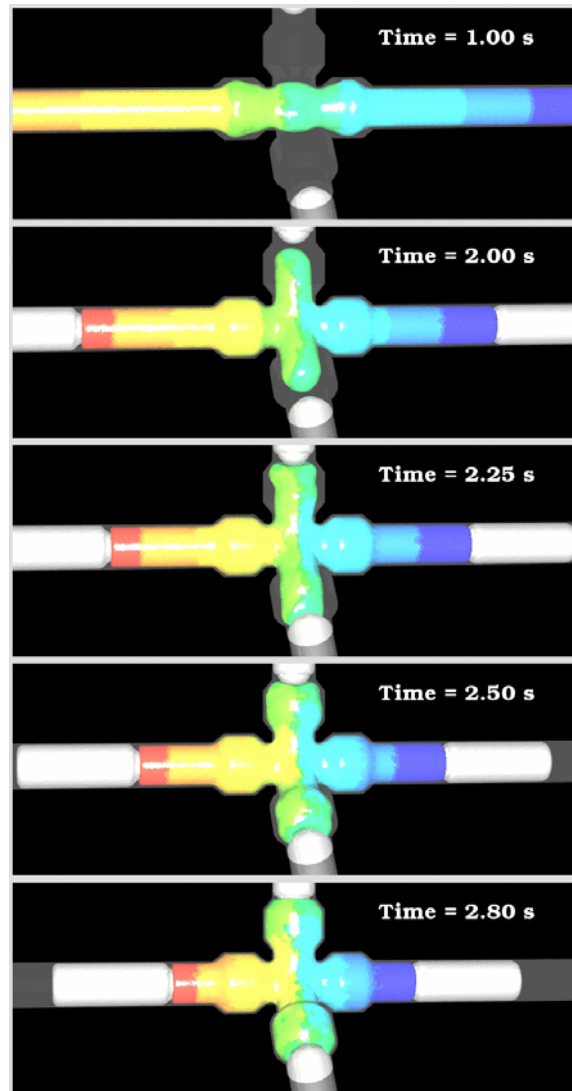

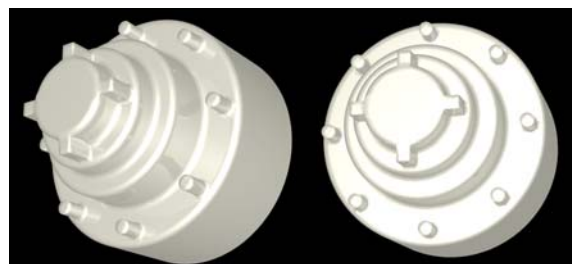**Figure 7:** Different stages of forging of component 1.

Figure 8: Die geometry for forging component 2.

Figure 9 shows the forging process as the piston compresses the blank into the die. The blank is again coloured by equal width strata to track deformation. Initially, the relative positions of these colour block are fairly constant. The pattern of material flow becomes more complex in regions of large deformation. At 0.25 s, part of the work piece intrudes into the region of the second cylinder from the top. As the cylinder is smaller than the work piece, material near the outer perimeter remains below the second cylinder. The material from the central region of the work piece is pushed up into the space of the second cylinder. Note the small amount of

cyan coloured material near the top at time 0.55 and 0.60 s. By 0.65 s, some material reaches the top cylinder. As the top cylinder has a smaller radius than that of the second cylinder, only material from the central region of the work piece reaches there. These geometric constrictions introduce resistance to the flow of material upwards and cause material to spread outward. By 0.7 s, material near the piston has spread out to the outer surface of the largest cylinder. Further on, material begins to fill the 8 pins and the + shaped extension on the top level. By 0.77 s, the forging is completed (see Figure 10).
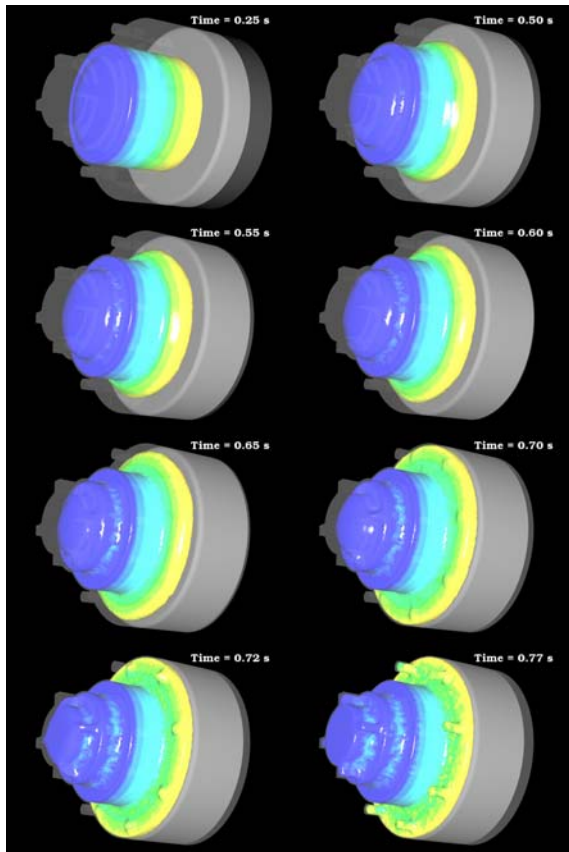
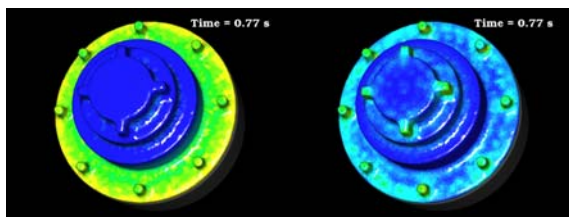

Figure 9: Different stages of forging of component 2.

Figure 10: Forged component 2 coloured (left) initial strata and (right) plastic strain, with blue for low value and yellow for high value.

DISCUSSION/CONCLUSION

In this paper we have demonstrated that SPH can be used to model the forging process and that insights can be gained into the nature of the solid metal flow, the overall deformation of different parts of the forging and the local deformation of the metal. SPH can directly predict several types of defects, such as incomplete die filling, inadequate forging pressure and flashing. It also has the potential to provide new types of information for forging optimisation because of its inherent history carrying capability, specifically direct predictions of defects such as:

- Surface Oxidation (scale) can form if the metal is heated too much prior to forging.
- Coarse Grain Structure: A final forging may contain coarse grains if the finishing temperature is too high or strain is too low adversely affecting mechanical properties. Local grain structure models can be easily implemented to predict these properties.
- Fracture: When deformation limits are exceeded due to excessive loads, material failure may occur in the work piece or dies. Explicit damage models can be easily included in SPH to allow direct prediction.
- Flash cracks: In flash regions rapid cooling, excessive pressures can build up in the work piece, resulting in cracks propagating into the bulk material.
- Lap Formation (or Cold Shuts): Poor material flow patterns lead to the metal folding over on itself forming weak seams that are pressed into the surface.

REFERENCES

BRAMLEY, A. N. and MYNORS, D. J., (2000), "The use of forging simulation tools", *Materials and Design*, **21**, 279-286.

CHO, J.R. and YANG, D.Y., (2000). "Three-dimensional finite element simulation of a spider hot forging process using a new remeshing scheme", *Journal of Materi als Processing Technology*, **99**, 219-225.

CLEARY, P.W., PRAKASH, M., HA, J., STOKES, N., and SCOTT, C., (2005), "Smoothed Particle Hydrodynamics; Status and future potential", Proc. 4th Int. Conf. on CFD in the Oil and Gas, Metallurgical & Process Industries, Norway, Eds. S.T. Johansen, I.G.

FERNANDEZ-MENDEZ, S., BONET, J. and HUERTA, A., (2005), "Continuous blending of SPH with finite elements", *Computers and Structures*, **83**, 1448-1458.

GRAY, J. P., MONAGHAN, J. J. and SWIFT, R. P., (2001), "SPH elastic dynamics", *Comput. Methods Appl. Mech. Engrg.*, **190**, 6641-6662.

LI, G. and BELYTSCHKO, T., (2000). "Element free Galerkin method for contact problems in metal forming analysis", *Engineering Computations*, **18**, 62-78.

LOF, J, (2000), "Developments in finite element simulations of aluminium extrusion", *PhD Thesis*, University of Twente, Netherlands.

MONAGHAN, J.J., (1992), "Smoothed particle hydrodynamics", *Ann. Rev. Astron. Astrophys.*, **30**, 543-574.

PRAKASH, M., CLEARY, P., GRANDFIELD, J., ROHAN, P. and NGUYEN, V., (2005), "Optimisation of ingot casting wheel design using SPH simulations", *Fourth Int. Conf. on CFD in the Oil and Gas, Metallurgical & Process Industries,* Trondheim, Norway.

TIERNAN, P., HILLERY, M. T., DRAGANESCU, B., and GHEORGHE, M., (2005), "Modelling of cold extrusion with experimental variation", *Journal of Materials Processing Technology*, **168**, 360-366.

WILKINS, J.L., (1964), "Calculation of Elastic-plastic Flow", *Methods of Computational Physics*, Academic Press, New York, **8**.